

Characterization of Exoplanets: Secondary Eclipses

Roi Alonso

Abstract When an exoplanet passes behind its host star, we can measure the time of the occultation, its depth, and its color. In this chapter we describe how these observables can be used to deduce physical characteristics of the planet such as its averaged dayside emission, departures from uniform disk illumination, or a precise measurement of the orbital eccentricity. This technique became a reality in 2005; in this chapter we describe the basics of the technique, its main results in the last 12 years, and the prospects for the years to come. This chapter includes a Table with references to all published detections of secondary eclipses until December 2017.

Introduction

One of the challenges to detect and characterise exoplanets is to distinguish their light from the much more intense and nearby source that is its host star. While several techniques can be used to resolve (i.e., separate) the images from the star and planet (see chapter “Direct Imaging as an Exoplanet Discovery Method” by L. Pueyo), in most of currently known exoplanets, and using state-of-the-art instrumentation, we are still far from being able to reach the required precision. Luckily, if the orbital configuration is favorable, there is one moment in the orbit of the exoplanet when we can infer the relative contribution of the light from a given exoplanet to the light of the combined stellar system: the secondary eclipses or occultations, the moment when the planet disappears behind its host star (Figure 1). A measure of the flux of the system that spans from moments before the secondary eclipse to moments after, can be immediately converted into the relative contribution of the light coming from exoplanet. Short period planets are especially prone to this type

Roi Alonso

Instituto de Astrofísica de Canarias, C. Vía Láctea S/N, E-38205 La Laguna, Tenerife, Spain, and
Departamento de Astrofísica de la Universidad de La Laguna, E-38206, La Laguna, Tenerife, Spain
e-mail: ras@iac.es

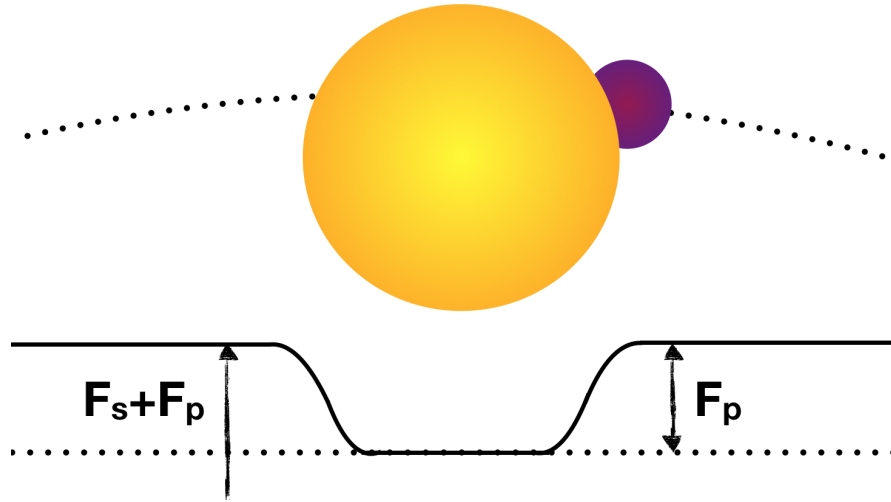


Fig. 1 Basic sketch of a secondary eclipse observation. By measuring the combined flux of the star and planet (F_s and F_p respectively) during a predicted secondary eclipse, we can isolate the contribution of the flux that is emitted and reflected by the planet.

of measurements, for several reasons: first, the closer they are to the host star, the larger the incident flux, and thus the reflected light and thermal emission, due to their temperatures of typically 1000-2000K. Second, the probability to produce eclipses is higher for short period planets, and the duration of these eclipses is of a few hours, which is a timescale that allows an observation during a single observing night, or, if observed from space, is not as expensive as other time consuming measurements like the orbital phase (see chapter “Exoplanet phase curves: observations and theory” by Parmentier & Crossfield). Finally, the rotation of the short period planets is thought to be synchronised with the orbital period, causing the same side of the planet to be monitored at every eclipse event. This alleviates the difficulty of the interpretation of the results, and means that, if the atmosphere is in equilibrium, we can re-observe the eclipse for several orbits to gain in significance of any detectable signal, as the observed distribution of light on the surface will not change.

Currently, secondary eclipse measurements of over 80 planets have been obtained from both ground and space-based observations. These have been compiled in Table 1, at the end of this chapter. There are mainly three quantities that we can measure during a secondary eclipse: the time when it occurs, its depth, and its wavelength dependence. We will describe what can be learned from each of these quantities in the next sections.

Timing of secondary eclipse and eclipse mapping

Once a transiting planet is known, in order to observe its secondary eclipse, the first important parameter is the time when it is expected to happen. For this, we need to know the eccentricity and orientation of its orbit, which can be extracted from radial velocity observations, or, as in the majority of the short periodic cases, we can make the reasonable assumption of a circular orbit and schedule the observations at half a period after a transit event. In reverse, the measurement of the time at which the eclipse happens carries information on the eccentricity of the orbit: given the period of the planet P , and the times of transit and secondary eclipse (t_1 and t_2 respectively), the relation that describes this (the tangential component of the eccentricity $e \cos \omega$) can be expressed (Kopal 1946):

$$e \cos \omega = \frac{\pi (t_2 - t_1 - \frac{P}{2})}{P (1 + \csc^2 i)} \quad (1)$$

where e is the eccentricity of the orbit, ω its argument of periastron, and i the orbital inclination. The radial component of the eccentricity, or $e \sin \omega$, can in principle be obtained from the duration of the transit and eclipse events (d_1 and d_2 , respectively):

$$e \sin \omega = \frac{d_2 \delta - d_1}{d_2 \delta + d_1} \quad (2)$$

where δ can be expressed as:

$$\delta = \sqrt{\frac{1 - (\frac{R_s}{R_p + R_s})^2 \cos^2 i}{1 - (\frac{R_p}{R_p + R_s})^2 \cos^2 i}} \quad (3)$$

and R_s and R_p are the radii of the star and planet, respectively. In practice, the radial component of the eccentricity is less precisely determined than the tangential component, as the times of the eclipses are easier to measure than their duration, and the constraints obtained by the radial velocities typically allow a more accurate determination of this component. Once combined, it is then possible to solve for the e and ω of the orbit, from which especially the eccentricity is an important parameter to test dynamical and tidal effects (e.g. Machalek et al 2010; Buhler et al 2016; Hardy et al 2017; Wilkins et al 2017), and it allows the study of heating rates and radiative timescales under different orbital configurations (Laughlin et al 2009; Cubillos et al 2013; Lewis et al 2014). The high accuracy on the eccentricity measurement, combined with precise radial velocities, has been suggested as a method to search for co-orbital bodies to known planets (Lillo-Box et al 2017).

Additionally, there is an expected timing offset, not included in the previous relations, due to the finite light speed and the time it takes to travel the $2 \times$ radius of the orbit (in the case of circular orbits) (e.g. Charbonneau et al 2005; Irwin 1959). For typical hot-Jupiters, with semi-major axes of about 0.01 AU, this is on the order of a few seconds.

If the eccentricity and argument of periastron of the orbit have been measured by other means to a high precision, and the mass of the host star is known, then the time for central eclipse can be predicted. Considering that these were accurate enough, and that the systematic noises were kept down to reasonable values, any departures from the measured times can then be ascribed to the effect of non-uniform illumination of the day-side of the planet (Williams et al 2006; Agol et al 2010; Dobbs-Dixon et al 2015). One possibility for this non-uniformity is an east-ward jet (where the ‘east’ is defined as the direction of planetary rotation) that has long been predicted from several atmospheric models (e.g. Showman and Guillot 2002; Cooper and Showman 2006; Cho et al 2003; Burkert et al 2005). This non-uniformity of the dayside produces changes in the ingress and egress profiles, which when fitted to a symmetrical eclipse model, leads to measured offsets of the time of central eclipse. If the precision of the data is high enough, and the ingress and egress are adequately sampled, it is possible to expand this technique and map the visible hemisphere of the planet (see chapter “Mapping exoplanets” by Cowan and Fujii).

Reflected light and thermal emission

The second important parameter that can be extracted from a secondary eclipse measurement is its depth, which gives the relative contribution of the flux coming from the planet to the light from the star F_p/F_s (Figure 1). In the most general case, the light that we receive from the planet is a combination of thermal emission and reflected light.

In the case when the reflected light is dominant, the depth of the eclipse can be expressed as:

$$\frac{F_p}{F_s} = A_g \left(\frac{R_p}{a} \right)^2 \phi(\alpha) \quad (4)$$

where A_g is the geometric albedo, R_p is the planetary radius, a the semi-major axis, and $\phi(\alpha)$ is the phase function, which for the case of a secondary eclipse, it can be approximated to 1 (i.e., the planetary disk appears fully illuminated).

In the alternative case of a planet whose emission is dominated by a thermal component (either reprocessed light from the stellar irradiation, or any source of internal heat), the observed eclipse depth is:

$$\frac{F_p}{F_s} = \frac{B(\lambda, T_{d,p})}{B(\lambda, T_s)} \left(\frac{R_p}{R_s} \right)^2 \quad (5)$$

where R_s is the radius of the star, and $B(\lambda, T_s)$ and $B(\lambda, T_{d,p})$ are the blackbody emissions of the star and the planetary dayside at brightness temperatures of T_s and $T_{d,p}$, respectively. In the case of the planet, this is a blackbody emission at the diurnal temperature, or a blackbody whose emission equals the total of the illuminated day-side of the planet. It should be noted that if the planet re-emission is non-isothermal,

different dayside locations will emit at different blackbody temperatures, and the resulting emission will not be a Planck curve. The sum of blackbodies emitting with different temperatures at concentric annuli, calculated from the dayside center toward the limb can provide a better description for the thermal re-emission, and if not taken into account, this can lead to underestimations of the thermal emission in the optical wavelengths (Schwartz and Cowan 2015). As in the more general scenario the observed eclipse depth will be a combination of reflected light and thermal emission (a sum of Eqs. 4 and 5), these estimations of the planet’s dayside temperature are necessary to extrapolate the thermal flux (typically measured in the near infrared) to the optical wavelengths, in order to isolate the contribution from the reflected light with the goal to measure the geometric albedo.

Following the formalism described in (Cowan and Agol 2011), we can define the equilibrium temperature of the sub-stellar point of the planet (also called ‘irradiation Temperature’ in some works) as:

$$T_0 = T_\star \sqrt{(R_\star/a)} \quad (6)$$

which can then be used to estimate the temperature of the planet, given its Bond albedo (A_B , or the fraction of all the incident flux from the star -at all wavelengths- that is absorbed by the planet) and a parametrisation of the efficiency of the transport of the incident flux from the sub-stellar point to the nightside. There are several slightly different ways to model this transport; still following (Cowan and Agol 2011), the dayside (T_d) and the nightside (T_n) effective temperatures can be estimated as:

$$T_d = T_0(1 - A_B)^{1/4} \left(\frac{2}{3} - \frac{5}{12}\epsilon \right)^{1/4} \quad (7)$$

$$T_n = T_0(1 - A_B)^{1/4} \left(\frac{\epsilon}{4} \right)^{1/4} \quad (8)$$

where the efficiency of the heat transport from the dayside to the nightside is represented by the factor ϵ . In this formulation, both A_B and ϵ have to take values from 0 to 1. The particular case with $A_B=0$ and $\epsilon=1$ is sometimes used to define an equilibrium temperature T_{eq} , listed in Table 1, and corresponding to $T_{eq} = T_0/\sqrt{2}$. Thus, in a system where we know the stellar parameters, and for a given Bond albedo, we can estimate with Eqs. 6 and 7 the dayside temperature. A comparison with the observed T_d from Eq. 5 can then serve in principle to estimate the efficiency factor ϵ , although solving the energy budget has revealed to be a challenging task (see e.g. Schwartz and Cowan 2015; Schwartz et al 2017, or the chapter “Exoplanet phase curves: observations and theory” by Parmentier & Crossfield).

Colours of the secondary eclipses

The third dimension that can be given to the measurements of a secondary eclipse is that of studying its wavelength dependence. As discussed in the previous section, in several cases it is difficult to distinguish what fraction of the light that we receive comes from reflection and what fraction is thermal emission. Extending the observations to different wavelengths can help alleviate this problem. At the near-infrared region most if not all the light received will be thermal emission, and in the bluest visible colors the light will be dominated by reflected light. Ideally, an observation at all the wavelengths would be needed to measure the Bond albedo (by definition a non-wavelength dependent parameter), and to study the geometric albedo at different colors. Moreover, knowing the dayside emission of a planet in different wavelengths allows it to be placed in color-color diagrams, or in color-magnitude once their distance is estimated by other means, and compare the current exoplanet sample to the more numerous brown dwarf/low mass stars at comparable effective temperatures (Triaud 2014; Triaud et al 2014).

Combining the data from narrower bands (commonly referred as bins), a low-resolution spectrum of the dayside emission starts to build up. This, as in the case of transmission spectra, will have imprinted features revealing the components of the atmosphere. The WFC3 on-board the HST has been used with great success to obtain emission spectra of half a dozen planets in the 1.1 - 1.7 μm spectral region (Table 1), providing measurements on up to 29 different spectral bins for the case of WASP-18b (Sheppard et al 2017). Both transmission and emission spectroscopy are described in detail in the chapter “Exoplanet Atmosphere Measurements from Transmission Spectroscopy and Other Planet Star Combined Light Observations” by L. Kreidberg.

Observations

In Table 1 we list the reported measurements until December 2017. A total of 83 exoplanets have reported secondary eclipse detections, and 65% of them have been detected in more than one wavelength. The majority of the reported detections come from the three space telescopes Spitzer, Hubble or Kepler, but 35% of the exoplanets have also been detected from the ground. The detection of the secondary eclipse of an exoplanet is a very challenging task: as shown in Figure 2, the depths in the most favorable cases of hot Jupiters observed in the near infrared are typically of a few tens of a percent. In the optical wavelengths, the measured depths, regardless of their origin (thermal or reflected light), are typically below 100 parts per million (ppm). The periods of the planets in which the detections have been possible are almost all below 10 d, the only exception being the 111 d period, highly eccentric planet HD 80606b (Laughlin et al 2009), whose secondary eclipse is close to periastron. Figure 3 shows an histogram of the orbital periods for the detections reported in Table 1, and Figure 4 the histograms of the planetary radii. The currently smallest

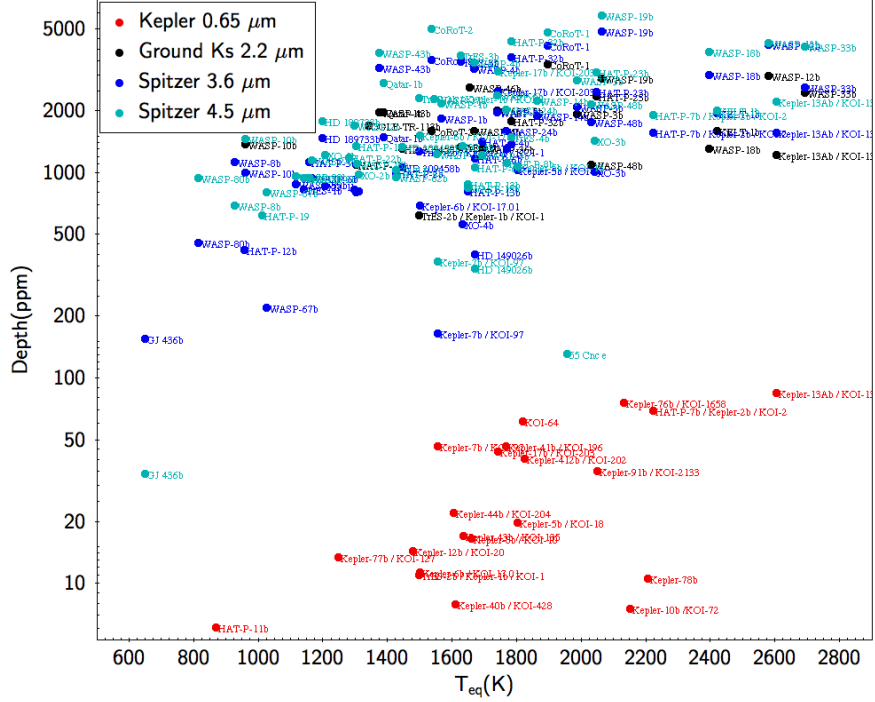


Fig. 2 Current (Dec 2017) sample of measured eclipses depths as a function of the equilibrium temperature. The different colors stand for measurements obtained with the most successful instrumentation: Spitzer in its two bluer colors (3.6 and 4.5 micron), Kepler, and ground-based measurements in the Ks filter. For a complete sample including other instrumentation and references please check Table 1.

planet radius of an object with a secondary eclipse detection is that of Kepler-78b (Sanchis-Ojeda et al 2013), thanks to its short orbital period of 0.36 d and observations in the 4 yr long main Kepler mission, highlighting the challenge of these observations. A few examples of observations of secondary eclipses with different instruments and analysis techniques is provided in Figure 5.

Observational highlights

In this section we highlight some of the works that made an important contribution to the development of this technique, and the (subjectively) most relevant observational results in a chronological order.

Early attempts Direct detections of the atmospheres of exoplanets were attempted from the ground soon after the first hot Jupiters were found, using high-resolution spectroscopy (Collier Cameron et al 1999, Charbonneau et al 1999) of non-transiting

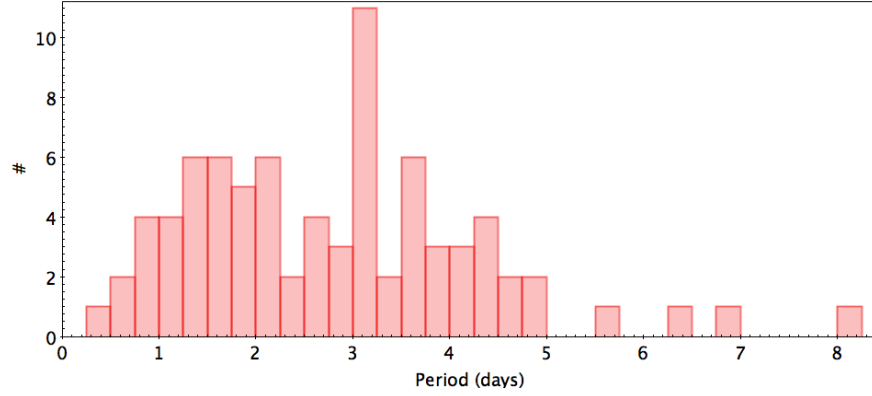


Fig. 3 Histogram of the periods of reported secondary eclipse measurements. For a complete list and references please check Table1.

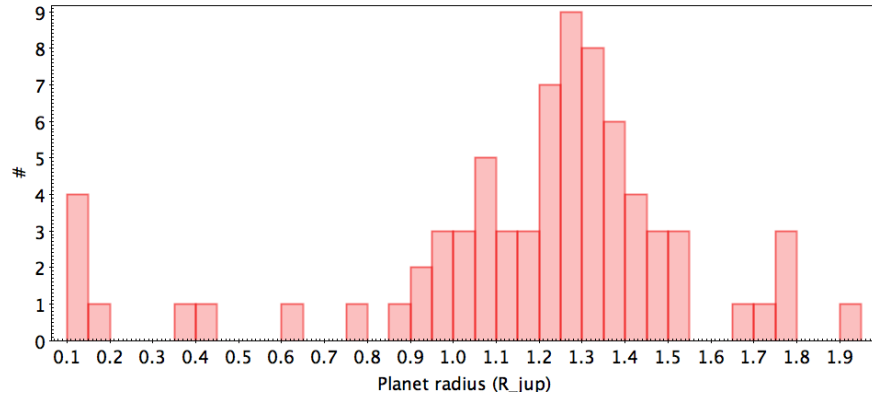


Fig. 4 Histogram of the radii of planets with reported secondary eclipse measurements. For a complete list and references please check Table1.

planets. Even if observations of non-transiting planets suffer from additional degenerate solutions due to the unknown orbital inclination, all these studies were performed before the first transiting planet was discovered (Charbonneau et al 2000; Henry et al 2000). Secondary eclipse detection was attempted soon after this discovery in the near-infrared using low-resolution spectroscopy (Richardson et al 2003b,a), or broad-band imaging (Snellen 2005). While these works pioneered the techniques that would succeed later, no firm detections were reported.

Secondary eclipse detections The first confirmed detections were reported with NASA’s Spitzer telescope (Deming et al 2005, Charbonneau et al 2005), for which it should be emphasised that it was not designed to perform these kind of observations. The two works reported a secondary eclipse of the first known exoplanet HD 209458b at $24\mu\text{m}$, and of TrES-1b at 3.6 and $4.5\mu\text{m}$, respectively. The impact

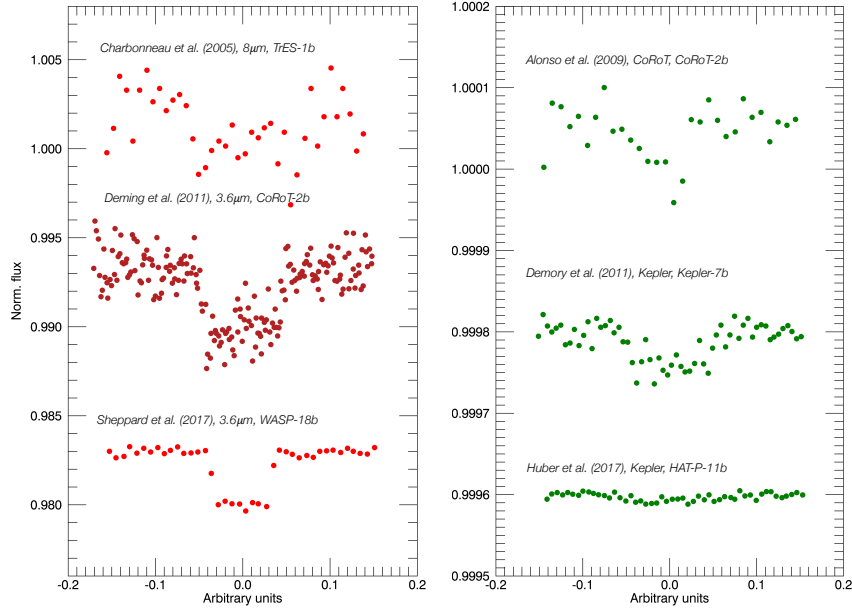


Fig. 5 Examples of observed secondary eclipses, showing the increase in precision in the last decade. The left panel shows secondary eclipses observed with Spitzer in the near-infrared, and the right panel in optical wavelengths with CoRoT and Kepler.

of the Spitzer telescope observations and its IRAC camera (Fazio et al 2004) in the years that followed has been enormous, as can be glimpsed from the Table 1 and Figure 2. Despite being a space-based observatory, there was a smooth learning curve to understand the impact of the systematic effects and to develop techniques to decorrelate the raw data obtained with this telescope (e.g., Todorov et al 2013; Deming et al 2015), a knowledge that was used later on to extract photometric light curves from the K2 mission (Luger et al 2016, 2017), and is expected to be of interest for future missions.

First secondary eclipses from the ground López-Morales and Seager (2007) explored the prospects for detections in the optical wavelengths of thermal emissions of hot Jupiters. Soon after, Sing and López-Morales (2009) reported on a z-band detection, and ground-based secondary eclipses have been widely observed since then, mainly in the near-infrared wavelengths (e.g. de Mooij and Snellen 2009, Alonso et al 2010, Anderson et al 2010, Croll et al 2010b, Martioli et al 2017 to name a few, see also the black points in Figure 2, and Table 1).

Secondary eclipses in the visible (MOST, CoRoT, Kepler) Going to bluer optical wavelengths, we expect secondary eclipses to be dominated by reflected light, which has proven to be more difficult to detect than the thermal re-emission. Out

of the different space missions that reached the required precision, MOST (Walker et al 2003) initially provided upper limits to secondary eclipse detections (Rowe et al 2008), while CoRoT (Baglin et al 2006) made the first detections of secondary eclipses from space (Snellen et al 2009, Alonso et al 2009b, Parviainen et al 2013). With the Kepler mission (Borucki et al 2010), it was soon demonstrated that the precision needed to detect the secondary eclipses was easily achieved (Borucki et al 2009), and eclipse depths as shallow as a few parts per million have been reported (Kipping and Spiegel 2011, Esteves et al 2013, Angerhausen et al 2015, Huber et al 2017). The red points in Figure 2 represent the Kepler detections. At the wavelengths of these missions, and the type of planets in which these were performed, a significant leak of thermal radiation into the optical wavelengths is expected, rendering the interpretation of the results and their implications to understand the global energy budgets a challenging task, as this contribution has to be estimated and subtracted to infer the reflected light component (Schwartz and Cowan 2015). In order to reach the smaller planet population, for which individual secondary eclipse detections might not reach the required signal to noise, several authors decided to combine curves of secondary eclipses from different small planets to gain statistical insights into different types of planets (Demory 2014, Jansen and Kipping 2017, Sheets and Deming 2017).

Secondary eclipses resolved in wavelength. By measuring the secondary eclipse depth in different wavelengths, we start to get low resolution spectra of the average dayside of the planet. This allows to alleviate the degeneracies between thermal and reflected light, and can in principle be used to sample the atmosphere of the planet at different pressure levels (e.g. Komacek et al 2017). Examples of multi-wavelength secondary eclipse observations are Charbonneau et al (2008) using 5 Spitzer bandpasses, Croll et al (2011) using 3 bandpasses from the ground, and Kreidberg et al (2014) using 15 different bands using HST/WFC3. Line et al (2014) performed a systematic retrieval analysis of secondary eclipse spectra of nine planets, presenting a catalogue of temperatures and abundances for four different molecules, and Shepard et al (2017) use a wide range secondary eclipse observations to constrain the C/O ratio and metallicity of WASP-18b, to cite a few examples.

Mapping The detailed shapes of the ingress and egress of the secondary eclipse carry valuable information that enables the mapping of the “surface” (or atmosphere) of the planet. This has been achieved with HD 189733b (Majeau et al 2012, de Wit et al 2012), and is described in detail in the chapter “Mapping Exoplanets” by N. Cowan and Y. Fujii.

Color-magnitude diagrams A traditional way to classify astronomical objects is by means of color-magnitude and color-color diagrams. Using the information from secondary eclipses in different band-passes, and the distances to the host star obtained through interferometry or photometric parallaxes, Triaud (2014) and Triaud et al (2014) reported on the location of known exoplanets into these diagrams. This allows to compare the emission of exoplanets with that of field brown dwarfs and

very low mass stars; the studied sample of 44 exoplanets appear to have a larger variety in color than brown dwarfs, and they do not match black-body emissions.

Love numbers When a planet is exposed to external forces, the elastic deformation response is quantified through its Love number (k_2) (Love 1909). Hot Jupiters in multiple planetary systems are particular cases in which an orbital eccentricity encodes information about the planet’s Love number, which itself enables to constrain the structure of the interior of the planet. The hot Jupiter HAT-P-13b was found to be part of a multiple planetary system (Bakos et al 2009), and precise timing of its secondary eclipses has allowed accurate measurements of its eccentricity, which was converted into estimations of the k_2 number (Batygin et al 2009). These lead to a measure of the core mass. Two independent studies (Buhler et al 2016; Hardy et al 2017), while reaching slightly inconsistent estimations of the Love number of planet *b*, $k_{2b} = 0.31^{+0.08}_{-0.05}$, and $k_{2b} = 0.81 \pm 0.10$, provide a demonstration of this method to probe the interior of extrasolar planets.

Caveats and prospects

As the observations of secondary eclipses are a challenging measurement, a good knowledge and/or control of instrumental systematic effects is mandatory for an accurate interpretation of the results and to avoid over-interpretations of the data. While less critical than in other longer-term observations such as phase curves, uncorrected systematic effects can lead to inconsistencies among the results obtained by different analysis techniques, showing that there is still room for improvement.

Even if the estimation of the brightness temperatures from the depth of the secondary eclipse might seem straightforward, solving for the global energy balance between the incident flux and the re-emission has proven to be a challenging task (Schwartz and Cowan 2015): first, it is necessary to separate, at a given wavelength, the contribution from reflected light and that from thermal emission of the planet. The fact that the disk of the illuminated planet has non-uniform temperatures (decreasing towards the limbs), further complicates the interpretation of the dayside brightness temperature. Fortunately, the degeneracies in the method (albedo vs. redistribution factor, or similar combinations under different formalisms) can be alleviated if observations at various wavelengths, accurate transit parameters and a complete phase curve can be obtained (see chapter “Exoplanet Phase Curves: Observations and Theory” by Parmentier & Crossfield). Finally, chemistry and clouds can affect the interpretation of even large and accurate sets of data, as further elaborated in that chapter (see also Heng and Demory 2013; Demory et al 2013; Parmentier et al 2016)

A quick look at Table 1 helps to understand that most of the observations of secondary eclipses has been achieved from space. Both HST and Spitzer are expected to keep observing secondary eclipses, and soon the methodology and experience acquired with these satellites will be applied to the upcoming JWST mission. With its

aperture of 6.5 m, JWST will observe some benchmark cases for different types of planets (Cowan et al 2015; Beichman et al 2014; Mollière et al 2016), while other upcoming space missions, TESS (Ricker 2014), CHEOPS (Broeg et al 2013) and PLATO (Rauer et al 2014), will find new benchmark planets. All the future space missions are more powerful when exploring their complementarities: TESS will observe preferentially the continuous viewing zones of JWST, while Gaidos et al (2017) proposed to use the slightly different throughputs of TESS and CHEOPS to disambiguate the thermal and reflected light contribution from a few hot Jupiters.

Ground-based observations are expected to keep increasing the performance of current observations, and extending it to higher resolution and fainter targets and/or smaller planets, with several 30 m telescopes on the horizon.

Together, in the next decade the number and quality of current observations is expected to increase significantly, revealing new correlations or trends, and testing and extending our current knowledge of the atmospheres of exoplanets.

Table 1: Current exoplanets with reported secondary eclipse measurements up to December 2017.

Planet	$T_{eq}(K)^a$	P (days)	$\lambda (\mu m)^b$	Refs. ^c
55 Cnc e	1958	0.74	4.5	1,2
CoRoT-1 b	1897	1.51	0.6, 0.71, 1.63, 2.10, 2.15, [3 – 9] 3.6, 4.5	
CoRoT-2 b	1537	1.74	0.6, 0.71, 2.15, 3.6, 4.5, 8	[10 – 14]
GJ 436 b	770	2.64	3.6, 4.5, 5.8, 8, 16, 24	[15 – 20]
HAT-P-1 b	1304	4.47	2.2, 3.6, 4.5, 5.8, 8	21,22
HAT-P-2 b	1427	5.63	3.6, 4.5, 5.8, 8	23
HAT-P-3 b	1157	2.90	3.6, 4.5	24
HAT-P-4 b	1693	3.06	3.6, 4.5	24
HAT-P-6 b	1671	3.85	3.6, 4.5	25
HAT-P-7b / Kepler-2b / KOI-2	2226	2.21	0.65, 3.6, 4.5, 5.8, 8	[26 – 34]
HAT-P-8 b	1771	3.08	3.6, 4.5	25
HAT-P-11 b	870	4.89	0.65	35
HAT-P-12 b	957	3.21	3.6, 4.5	24
HAT-P-13 b	1649	2.92	3.6, 4.5	36,37
HAT-P-19 b		4.01	3.6, 4.5	38
HAT-P-22 b	1280	3.21	4.5	39
HAT-P-23 b	2047	1.21	2.2, 3.6, 4.5	40
HAT-P-32 b	1783	2.15	1.63, 2.2, 3.6, 4.5	41
HD 149026 b	1645	2.88	3.6, 4.5, 5.8, 8, 16	42, 43
HD 189733 b	1198	2.22	[1.1-1.7], [1.5-2.5], 2.2, [2-2.4],[3.1-4.1],3.6,4.5, 5.8,8, [5-14],[7.5-14.7], 16	[44 – 56]

Table 1: (Continued)

Planet	$T_{eq}(K)^a$	P (days)	λ (μm)	Refs.
HD 209458 b	1445	3.52	0.6, [1.1-1.7], 1.65, 2.2, 3.5, [57 – 71] 3.6, 3.8, 4.5, 5.8, 8, [7.5 - 15.3], 24	
HD 80606 b	397	111.44	8	72
KELT-1 b	2422	1.22	0.9, 2.2, 3.6, 4.5	73, 74
Kepler-5b / KOI-18	1804	3.55	0.65, 3.6, 4.5	75, 29, 31, 32, 33
Kepler-6b / KOI-17	1502	3.24	0.65, 3.6, 4.5	75, 31, 32, 33
Kepler-7b / KOI-97	1630	4.89	0.65, 3.6, 4.5	76, 29, 77, 32, 33, 78
Kepler-8b / KOI-10	1680	3.52	0.65	31, 32, 33
Kepler-10b / KOI-72	2120	0.84	0.65	79, 32
Kepler-12b / KOI-20	1480	4.44	0.65	80, 32, 33, 78
Kepler-13Ab / KOI- 13	2606	1.76	0.65, [1.1-1.7], 2.2, 3.6, 4.5	81, 29, 31, 82, 32, 33, 83
Kepler-17b / KOI- 203	1743	1.49	0.65, 3.6, 4.5	84, 85, 33
Kepler-40b / KOI- 428	1611	6.87	0.65	33
Kepler-41b / KOI- 196	1770	1.86	0.65	86, 29, 32, 33, 78
Kepler-43b / KOI- 135	1635	3.02	0.65	32, 33
Kepler-44b / KOI- 204	1604	3.25	0.65	33
Kepler-76b / KOI- 1658	2140	1.55	0.65	87, 32, 33
Kepler-77b / KOI- 127	1247	3.58	0.65	33
Kepler-78b	2206	0.36	0.65	88
Kepler-91b / KOI- 2133	2051	6.25	0.65	32, 33, 89, 90
Kepler-93b / KOI-69		4.7	0.65	91, 92
Kepler-412b / KOI- 202	1826	1.72	0.65	93, 29, 32, 33
Kepler-423b	1411	2.68	0.65	94
KOI-1169.01		0.69	0.65	92
KOI-64	1820	1.95	0.65	29, 31
OGLE-TR-56b	2203	1.21	0.9	95
OGLE-TR-113b	1342	1.43	2.2	96

Table 1: (Continued)

Planet	$T_{eq}(K)^a$	P (days)	λ (μm)	Refs.
Qatar-1b	1387	1.42	2.2, 3.6, 4.5	74, 97, 98
TrES-1b	1142	3.03	3.5, 3.6, 4.5, 5.8, 8, 16	[99 – 101]
TrES-2b / Kepler-1b	1497	2.47	0.65, 2.2, 3.6, 4.5, 5.8, 8	[102 – 104],
/ KOI-1				31, 32, 33
TrES-3b	1627	1.31	0.66, 0.8, 0.9, 1.6, 2.2, 3.6, [105 – 108]	
			4.5, 5.8, 8	
TrES-4b	1784	3.55	3.6, 4.5, 5.8, 8	109
WASP-1b	1568	2.52	3.6, 4.5, 5.8, 8	110
WASP-2b	1298	2.15	2.2, 3.6, 4.5, 5.8, 8	110, 111
WASP-3b	1988	1.85	2.2, 3.6, 4.5, 8	112, 113, 74
WASP-4b	1669	1.34	2.2, 3.6, 4.5	114, 115, 111
WASP-5b	1740	1.63	1.2, 2.2, 3.6, 4.5	116, 117, 111
WASP-6b		3.36	3.6, 4.5	118
WASP-8b	926	8.16	3.6, 4.5, 8	119
WASP-10b	961	3.09	2.2, 3.6, 4.5	120, 118
WASP-12b	2581	1.09	0.45, 0.9, 1.02, 1.22, 1.63, [121 – 124],	
			2.2, 3.6, 4.5, 5.8, 8	8, 125, 126,
				74, 127
WASP-13b	1552	4.35	4.5	39
WASP-14b	1863	2.24	3.6, 4.5, 8	[128 – 130]
WASP-15b	1650	3.75	4.5	39
WASP-16b	1306	3.12	4.5	39
WASP-17b	1546	3.74	4.5, 8	131
WASP-18b	2395	0.94	[1.1-1.7], 2.2, 3.6, 4.5, 5.8, [132 – 134],	
			8	111
WASP-19b	2064	0.79	0.69, 0.8, 0.9, 1.19, 1.6, [135 – 144]	
			2.09, 2.2, 3.6, 4.5, 5.8, 8	
WASP-24b	1768	2.34	3.6, 4.5	145
WASP-33b	2692	1.22	0.91, 1.05, 2.2, 3.6, 4.5	[146 – 149]
WASP-36b	1697	1.54	2.2	111
WASP-39b		4.06	3.6, 4.5	38
WASP-43b	1374	0.81	0.8, [1.1-1.7] 1.6, 2.2, 3.6, [150–155],	
			4.5	143
WASP-46b	1656	1.43	1.2, 1.6, 2.2	156, 111
WASP-48b	2031	2.14	1.6, 2.2, 3.6, 4.5	40
WASP-62b	1426	4.41	4.5	39
WASP-67b		4.61	3.6, 4.5	38
WASP-76b		1.81	2.2	111
WASP-80b	814	3.07	3.6, 4.5	157
WASP-103b	2503	0.93	[1.1-1.7]	158

Table 1: (Continued)

Planet	$T_{eq}(K)^a$	P (days)	λ (μm)	Refs.
XO-1b	1206	3.94	3.6, 4.5, 5.8, 8	159
XO-2b	1312	2.62	3.6, 4.5, 5.8, 8	160
XO-3b	2043	3.19	3.6, 4.5, 5.8, 8	161
XO-4b		4.13	3.6, 4.5	25

^aDefined as $T_{eq} = T_{star} \sqrt{\frac{R_{star}}{2a}} = T_0/\sqrt{2}$

^b Wavelengths given in brackets mean that there are several measurements in that region, typically obtained by combining different wavelengths of low resolution spectra into different bins.

^c [1] Demory et al (2012), [2] Demory et al (2016), [3] Alonso et al (2009a), [4] Snellen et al (2009), [5] Rogers et al (2009), [6] Gillon et al (2009), [7] Deming et al (2011), [8] Zhao et al (2012b), [9] Parviainen et al (2013), [10] Alonso et al (2009b), [11] Snellen et al (2010), [12] Alonso et al (2010), [13] Gillon et al (2010), [14] Deming et al (2011), [15] Deming et al (2007a), [16] Stevenson et al (2010), [17] Beaulieu et al (2011), [18] Knutson et al (2011), [19] Lanotte et al (2014), [20] Morley et al (2017), [21] Todorov et al (2010), [22] de Mooij et al (2011), [23] Lewis et al (2013), [24] Todorov et al (2013), [25] Todorov et al (2012), [26] Borucki et al (2009), [27] Welsh et al (2010), [28] Christiansen et al (2010), [29] Coughlin and López-Morales (2012), [30] Morris et al (2013), [31] Esteves et al (2013), [32] Esteves et al (2015), [33] Angerhausen et al (2015), [34] Wong et al (2016), [35] Huber et al (2017), [36] Buhler et al (2016), [37] Hardy et al (2017), [38] Kammer et al (2015), [39] Kilpatrick et al (2017), [40] O'Rourke et al (2014), [41] Zhao et al (2014), [42] Knutson et al (2009b), [43] Stevenson et al (2012), [44] Deming et al (2006), [45] Grillmair et al (2007), [46] Barnes et al (2007), [47] Knutson et al (2007a), [48] Charbonneau et al (2008), [49] Grillmair et al (2008), [50] Knutson et al (2009c), [51] Swain et al (2009b), [52] Agol et al (2010), [53] Swain et al (2010), [54] Knutson et al (2012), [55] Todorov et al (2014), [56] Crouzet et al (2014), [57] Deming et al (2005), [58] Richardson et al (2003b), [59] Richardson et al (2003a), [60] Snellen (2005), [61] Deming et al (2007b), [62] Swain et al (2009b), [63] Knutson et al (2008), [64] Rowe et al (2008), [65] Swain et al (2009a), [66] Crossfield et al (2012b), [67] Diamond-Lowe et al (2014), [68] Zellem et al (2014b), [69] Zellem et al (2014a), [70] Evans et al (2015), [71] Line et al (2016), [72] Laughlin et al (2009), [73] Beatty et al (2014), [74] Croll et al (2015), [75] Désert et al (2011b), [76] Demory et al (2011), [77] Demory et al (2013), [78] Shporer and Hu (2015), [79] Batalha et al (2011), [80] Fortney et al (2011), [81] Mazeh et al (2012), [82] Shporer et al (2014), [83] Beatty et al (2017), [84] Désert et al (2011a), [85] Bonomo et al (2012), [86] Santerne et al (2011), [87] Faigler et al (2013), [88] Sanchis-Ojeda et al (2013), [89] Barclay et al (2015), [90] Sato et al (2015), [91] Barclay et al (2015), [92] Demory (2014), [93] Deleuil et al (2014), [94] Gandolfi et al (2015), [95] Sing and López-Morales (2009), [96] Snellen and Covino (2007), [97] Cruz et al (2016), [98] Garhart et al (2017), [99] Charbonneau et al (2005), [100] Knutson et al (2007b), [101] Cubillos et al (2014), [102] Croll et al (2010a), [103] O'Donovan et al (2010), [104] Kipping and Spiegel (2011), [105] Winn et al (2008), [106] de Mooij and Snellen (2009), [107] Fressin et al (2010), [108] Croll et al (2010b), [109] Knutson et al (2009a), [110] Wheatley et al (2010), [111] Zhou et al (2015), [112] Zhao et al (2012a), [113] Rostron et al (2014), [114] Cáceres et al (2011), [115] Beerer et al (2011), [116] Baskin et al (2013), [117] Chen et al (2014a), [118] Kammer et al (2015), [119] Cubillos et al (2013), [120] Cruz et al (2015), [121] López-Morales et al (2010), [122] Croll et al (2011), [123] Campo et al (2011), [124] Crossfield et al (2012a), [125] Föhring et al (2013), [126] Stevenson et al (2014a), [127] Bell et al (2017), [128] Blecic et al (2013), [129] Wong et al (2015), [130] Krick et al (2016), [131] Anderson et al (2011), [132] Nymeyer et al (2011), [133] Maxted et al (2013), [134] Sheppard et al (2017), [135] Anderson et al (2010)), [136] Gibson et al (2010), [137] Burton et al (2012),

[138] Zhou et al (2013), [139] Lendl et al (2013), [140] Abe et al (2013), [141] Anderson et al (2013), [142] Mancini et al (2013), [143] Zhou et al (2014), [144] Wong et al (2016), [145] Smith et al (2012), [146] Smith et al (2011), [147] Deming et al (2012), [148] de Mooij et al (2013), [149] von Essen et al (2015), [150] Wang et al (2013), [151] Stevenson et al (2014b), [152] Chen et al (2014b), [153] Blecic et al (2014), [154] Kreidberg et al (2014) [155] Stevenson et al (2017), [156] Chen et al (2014c), [157] Triaud et al (2015), [158] Cartier et al (2017), [159] Machalek et al (2008), [160] Machalek et al (2009), [161] Machalek et al (2010).

Cross-References

- Mapping Exoplanets
- Exoplanet Phase Curves: Observations and Theory
- Exoplanet Atmosphere Measurements from Transmission Spectroscopy and other planet star combined light observations
- Direct Imaging as an Exoplanet Discovery Method

Acknowledgements The author acknowledges Hans Deeg for a revision of this chapter and fruitful discussions, and the Spanish Ministry of Economy and Competitiveness (MINECO) for the financial support under the Ramón y Cajal program RYC-2010-06519, and the program RETOS ESP2014-57495-C2-1-R and ESP2016-80435-C2-2-R. This contribution has benefited from the use of Topcat (<http://www.starlink.ac.uk/topcat/>), exoplanets.org, exoplanets.eu, and the author acknowledges the people behind these tools for their work.

References

- Abe L, Gonçalves I, Agabi A et al (2013) The secondary eclipses of WASP-19b as seen by the ASTEP 400 telescope from Antarctica. *A&A*553:A49
- Agol E, Cowan NB, Knutson HA et al (2010) The Climate of HD 189733b from Fourteen Transits and Eclipses Measured by Spitzer. *ApJ*721:1861–1877
- Alonso R, Alapini A, Aigrain S et al (2009a) The secondary eclipse of CoRoT-1b. *A&A*506:353–358
- Alonso R, Guillot T, Mazeh T et al (2009b) The secondary eclipse of the transiting exoplanet CoRoT-2b. *A&A*501:L23–L26
- Alonso R, Deeg HJ, Kabath P, Rabus M (2010) Ground-based Near-infrared Observations of the Secondary Eclipse of CoRoT-2b. *AJ*139:1481–1485
- Anderson DR, Gillon M, Maxted PFL et al (2010) H-band thermal emission from the 19-h period planet WASP-19b. *A&A*513:L3
- Anderson DR, Smith AMS, Lanotte AA et al (2011) Thermal emission at 4.5 and 8 μm of WASP-17b, an extremely large planet in a slightly eccentric orbit. *MNRAS*416:2108–2122
- Anderson DR, Smith AMS, Madhusudhan N et al (2013) Thermal emission at 3.6–8 μm from WASP-19b: a hot Jupiter without a stratosphere orbiting an active star. *MNRAS*430:3422–3431
- Angerhausen D, DeLarme E, Morse JA (2015) A Comprehensive Study of Kepler Phase Curves and Secondary Eclipses: Temperatures and Albedos of Confirmed Kepler Giant Planets. *PASP*127:1113

- Baglin A, Auvergne M, Boissard L et al (2006) CoRoT: a high precision photometer for stellar evolution and exoplanet finding. In: 36th COSPAR Scientific Assembly, COSPAR Meeting, vol 36
- Bakos GÁ, Howard AW, Noyes RW et al (2009) HAT-P-13b,c: A Transiting Hot Jupiter with a Massive Outer Companion on an Eccentric Orbit. *ApJ*707:446–456
- Barclay T, Endl M, Huber D et al (2015) Radial Velocity Observations and Light Curve Noise Modeling Confirm that Kepler-91b is a Giant Planet Orbiting a Giant Star. *ApJ*800:46
- Barnes JR, Barman TS, Prato L et al (2007) Limits on the 2.2- μ m contrast ratio of the close-orbiting planet HD 189733b. *MNRAS*382:473–480
- Baskin NJ, Knutson HA, Burrows A et al (2013) Secondary Eclipse Photometry of the Exoplanet WASP-5b with Warm Spitzer. *ApJ*773:124
- Batalha NM, Borucki WJ, Bryson ST et al (2011) Kepler's First Rocky Planet: Kepler-10b. *ApJ*729:27
- Batygin K, Bodenheimer P, Laughlin G (2009) Determination of the Interior Structure of Transiting Planets in Multiple-Planet Systems. *ApJ*704:L49–L53
- Beatty TG, Collins KA, Fortney J et al (2014) Spitzer and z' Secondary Eclipse Observations of the Highly Irradiated Transiting Brown Dwarf KELT-1b. *ApJ*783:112
- Beatty TG, Madhusudhan N, Tsias A et al (2017) Evidence for Atmospheric Cold-trap Processes in the Noninverted Emission Spectrum of Kepler-13Ab Using HST/WFC3. *AJ*154:158
- Beaulieu JP, Tinetti G, Kipping DM et al (2011) Methane in the Atmosphere of the Transiting Hot Neptune GJ436B? *ApJ*731:16
- Beier IM, Knutson HA, Burrows A et al (2011) Secondary Eclipse Photometry of WASP-4b with Warm Spitzer. *ApJ*727:23
- Beichman C, Benneke B, Knutson H et al (2014) Observations of Transiting Exoplanets with the James Webb Space Telescope (JWST). *PASP*126:1134
- Bell TJ, Nikolov N, Cowan NB et al (2017) The Very Low Albedo of WASP-12b from Spectral Eclipse Observations with Hubble. *ApJ*847:L2
- Blecic J, Harrington J, Madhusudhan N et al (2013) Thermal Emission of WASP-14b Revealed with Three Spitzer Eclipses. *ApJ*779:5
- Blecic J, Harrington J, Madhusudhan N et al (2014) Spitzer Observations of the Thermal Emission from WASP-43b. *ApJ*781:116
- Bonomo AS, Hébrard G, Santerne A et al (2012) SOPHIE velocimetry of Kepler transit candidates. V. The three hot Jupiters KOI-135b, KOI-204b, and KOI-203b (alias Kepler-17b). *A&A*538:A96
- Borucki WJ, Koch D, Jenkins J et al (2009) Kepler's Optical Phase Curve of the Exoplanet HAT-P-7b. *Science* 325:709
- Borucki WJ, Koch D, Basri G et al (2010) Kepler Planet-Detection Mission: Introduction and First Results. *Science* 327:977
- Broeg C, Fortier A, Ehrenreich D et al (2013) CHEOPS: A transit photometry mission for ESA's small mission programme. In: European Physical Journal Web of Conferences, European Physical Journal Web of Conferences, vol 47, p 03005, DOI 10.1051/epjconf/20134703005, 1305.2270
- Buhler PB, Knutson HA, Batygin K et al (2016) Dynamical Constraints on the Core Mass of Hot Jupiter HAT-P-13b. *ApJ*821:26
- Burkert A, Lin DNC, Bodenheimer PH, Jones CA, Yorke HW (2005) On the Surface Heating of Synchronously Spinning Short-Period Jovian Planets. *ApJ*618:512–523
- Burton JR, Watson CA, Littlefair SP et al (2012) z'-band Ground-based Detection of the Secondary Eclipse of WASP-19b. *ApJS*201:36
- Cáceres C, Ivanov VD, Minniti D et al (2011) A ground-based K_S-band detection of the thermal emission from the transiting exoplanet WASP-4b. *A&A*530:A5
- Campo CJ, Harrington J, Hardy RA et al (2011) On the Orbit of Exoplanet WASP-12b. *ApJ*727:125
- Cartier KMS, Beatty TG, Zhao M et al (2017) Near-infrared Emission Spectrum of WASP-103b Using Hubble Space Telescope/Wide Field Camera 3. *AJ*153:34

- Charbonneau D, Noyes RW, Korzennik SG et al (1999) An Upper Limit on the Reflected Light from the Planet Orbiting the Star τ Bootis. *ApJ*522:L145–L148
- Charbonneau D, Brown TM, Latham DW Mayor M (2000) Detection of Planetary Transits Across a Sun-like Star. *ApJ*529:L45–L48
- Charbonneau D, Allen LE, Megeath ST et al (2005) Detection of Thermal Emission from an Extrasolar Planet. *ApJ*626:523–529
- Charbonneau D, Knutson HA, Barman T et al (2008) The Broadband Infrared Emission Spectrum of the Exoplanet HD 189733b. *ApJ*686:1341–1348
- Chen G, van Boekel R, Madhusudhan N et al (2014a) Ground-based detection of the near-infrared emission from the dayside of WASP-5b. *A&A*564:A6
- Chen G, van Boekel R, Wang H et al (2014b) Broad-band transmission spectrum and K-band thermal emission of WASP-43b as observed from the ground. *A&A*563:A40
- Chen G, van Boekel R, Wang H et al (2014c) Observed spectral energy distribution of the thermal emission from the dayside of jASTROBJ_i WASP-46b/ ASTROBJ_i . *A&A*567:A8
- Cho JYK, Menou K, Hansen BMS Seager S (2003) The Changing Face of the Extrasolar Giant Planet HD 209458b. *ApJ*587:L117–L120
- Christiansen JL, Ballard S, Charbonneau D et al (2010) Studying the Atmosphere of the Exoplanet HAT-P-7b Via Secondary Eclipse Measurements with EPOXI, Spitzer, and Kepler. *ApJ*710:97–104
- Collier Cameron A, Horne K, Penny A James D (1999) Probable detection of starlight reflected from the giant planet orbiting τ Boötis. *Nature*402:751–755
- Cooper CS Showman AP (2006) Dynamics and Disequilibrium Carbon Chemistry in Hot Jupiter Atmospheres, with Application to HD 209458b. *ApJ*649:1048–1063
- Coughlin JL López-Morales M (2012) A Uniform Search for Secondary Eclipses of Hot Jupiters in Kepler Q2 Light Curves. *AJ*143:39
- Cowan NB Agol E (2011) The Statistics of Albedo and Heat Recirculation on Hot Exoplanets. *ApJ*729:54
- Cowan NB, Greene T, Angerhausen D et al (2015) Characterizing Transiting Planet Atmospheres through 2025. *PASP*127:311
- Croll B, Albert L, Lafreniere D, Jayawardhana R Fortney JJ (2010a) Near-Infrared Thermal Emission from the Hot Jupiter TrES-2b: Ground-based Detection of the Secondary Eclipse. *ApJ*717:1084–1091
- Croll B, Jayawardhana R, Fortney JJ, Lafrenière D Albert L (2010b) Near-infrared Thermal Emission from TrES-3b: A Ks-band Detection and an H-band Upper Limit on the Depth of the Secondary Eclipse. *ApJ*718:920–927
- Croll B, Lafreniere D, Albert L et al (2011) Near-infrared Thermal Emission from WASP-12b: Detections of the Secondary Eclipse in Ks, H, and J. *AJ*141:30
- Croll B, Albert L, Jayawardhana R et al (2015) Near-infrared Thermal Emission Detections of a Number of Hot Jupiters and the Systematics of Ground-based Near-infrared Photometry. *ApJ*802:28
- Crossfield IJM, Hansen BMS Barman T (2012a) Ground-based, Near-infrared Exospectroscopy. II. Tentative Detection of Emission from the Extremely Hot Jupiter WASP-12b. *ApJ*746:46
- Crossfield IJM, Knutson H, Fortney J et al (2012b) Spitzer/MIPS 24 μm Observations of HD 209458b: Three Eclipses, Two and a Half Transits, and a Phase Curve Corrupted by Instrumental Sensitivity Variations. *ApJ*752:81
- Crouzet N, McCullough PR, Deming D Madhusudhan N (2014) Water Vapor in the Spectrum of the Extrasolar Planet HD 189733b. II. The Eclipse. *ApJ*795:166
- Cruz P, Barrado D, Lillo-Box J et al (2015) Detection of the secondary eclipse of WASP-10b in the Ks-band. *A&A*574:A103
- Cruz P, Barrado D, Lillo-Box J et al (2016) Detection of the secondary eclipse of Qatar-1b in the Ks band. *A&A*595:A61
- Cubillos P, Harrington J, Madhusudhan N et al (2013) WASP-8b: Characterization of a Cool and Eccentric Exoplanet with Spitzer. *ApJ*768:42

- Cubillos P, Harrington J, Madhusudhan N et al (2014) A Spitzer Five-band Analysis of the Jupiter-sized Planet TrES-1. *ApJ*797:42
- de Mooij EJW, Snellen IAG (2009) Ground-based K-band detection of thermal emission from the exoplanet TrES-3b. *A&A*493:L35–L38
- de Mooij EJW, de Kok RJ, Nefs SV Snellen IAG (2011) The GROUSE project. II. Detection of the K_s -band secondary eclipse of exoplanet HAT-P-1b. *A&A*528:A49
- de Mooij EJW, Brogi M, de Kok RJ et al (2013) The GROUSE project. III. K_s -band observations of the thermal emission from WASP-33b. *A&A*550:A54
- de Wit J, Gillon M, Demory BO, Seager S (2012) Towards consistent mapping of distant worlds: secondary-eclipse scanning of the exoplanet HD 189733b. *A&A*548:A128
- Deleuil M, Almenara JM, Santerne A et al (2014) SOPHIE velocimetry of Kepler transit candidates XI. Kepler-412 system: probing the properties of a new inflated hot Jupiter. *A&A*564:A56
- Deming D, Seager S, Richardson LJ, Harrington J (2005) Infrared radiation from an extrasolar planet. *Nature*434:740–743
- Deming D, Harrington J, Seager S, Richardson LJ (2006) Strong Infrared Emission from the Extrasolar Planet HD 189733b. *ApJ*644:560–564
- Deming D, Harrington J, Laughlin G et al (2007a) Spitzer Transit and Secondary Eclipse Photometry of GJ 436b. *ApJ*667:L199–L202
- Deming D, Richardson LJ, Harrington J (2007b) 3.8- μ m photometry during the secondary eclipse of the extrasolar planet HD209458b. *MNRAS*378:148–152
- Deming D, Knutson H, Agol E et al (2011) Warm Spitzer Photometry of the Transiting Exoplanets CoRoT-1 and CoRoT-2 at Secondary Eclipse. *ApJ*726:95
- Deming D, Fraine JD, Sada PV et al (2012) Infrared Eclipses of the Strongly Irradiated Planet WASP-33b, and Oscillations of Its Host Star. *ApJ*754:106
- Deming D, Knutson H, Kammer J et al (2015) Spitzer Secondary Eclipses of the Dense, Modestly-irradiated, Giant Exoplanet HAT-P-20b Using Pixel-level Decorrelation. *ApJ*805:132
- Demory BO (2014) The Albedos of Kepler's Close-in Super-Earths. *ApJ*789:L20
- Demory BO, Seager S, Madhusudhan N et al (2011) The High Albedo of the Hot Jupiter Kepler-7b. *ApJ*735:L12
- Demory BO, Gillon M, Seager S et al (2012) Detection of Thermal Emission from a Super-Earth. *ApJ*751:L28
- Demory BO, de Wit J, Lewis N et al (2013) Inference of Inhomogeneous Clouds in an Exoplanet Atmosphere. *ApJ*776:L25
- Demory BO, Gillon M, Madhusudhan N, Queloz D (2016) Variability in the super-Earth 55 Cnc e. *MNRAS*455:2018–2027
- Désert JM, Charbonneau D, Demory BO et al (2011a) The Hot-Jupiter Kepler-17b: Discovery, Obliquity from Stroboscopic Starspots, and Atmospheric Characterization. *ApJS*197:14
- Désert JM, Charbonneau D, Fortney JJ et al (2011b) The Atmospheres of the Hot-Jupiters Kepler-5b and Kepler-6b Observed during Occultations with Warm-Spitzer and Kepler. *ApJS*197:11
- Diamond-Lowe H, Stevenson KB, Bean JL, Line MR, Fortney JJ (2014) New Analysis Indicates No Thermal Inversion in the Atmosphere of HD 209458b. *ApJ*796:66
- Dobbs-Dixon I, Agol E, Deming D (2015) Spectral Eclipse Timing. *ArXiv e-prints*
- Esteves LJ, De Mooij EJW, Jayawardhana R (2013) Optical Phase Curves of Kepler Exoplanets. *ApJ*772:51
- Esteves LJ, De Mooij EJW, Jayawardhana R (2015) Changing Phases of Alien Worlds: Probing Atmospheres of Kepler Planets with High-precision Photometry. *ApJ*804:150
- Evans TM, Aigrain S, Gibson N et al (2015) A uniform analysis of HD 209458b Spitzer/IRAC light curves with Gaussian process models. *MNRAS*451:680–694
- Faigler S, Tal-Or L, Mazeh T, Latham DW, Buchhave LA (2013) BEER Analysis of Kepler and CoRoT Light Curves. I. Discovery of Kepler-76b: A Hot Jupiter with Evidence for Superrotation. *ApJ*771:26
- Fazio GG, Hora JL, Allen LE et al (2004) The Infrared Array Camera (IRAC) for the Spitzer Space Telescope. *ApJS*154:10–17

- Föhring D, Dhillon VS, Madhusudhan N et al (2013) ULTRACAM z' -band detection of the secondary eclipse of WASP-12b. *MNRAS*435:2268–2273
- Fortney JJ, Demory BO, Désert JM et al (2011) Discovery and Atmospheric Characterization of Giant Planet Kepler-12b: An Inflated Radius Outlier. *ApJS*197:9
- Fressin F, Knutson HA, Charbonneau D et al (2010) The Broadband Infrared Emission Spectrum of the Exoplanet TrES-3. *ApJ*711:374–379
- Gaidos E, Kitzmann D Heng K (2017) Exoplanet Characterization by Multi-Observatory Transit Photometry with TESS and CHEOPS. *ArXiv e-prints*
- Gandolfi D, Parviainen H, Deeg HJ et al (2015) Kepler-423b: a half-Jupiter mass planet transiting a very old solar-like star. *A&A*576:A11
- Garhart E, Deming D, Mandell A, Knutson H Fortney JJ (2017) Spitzer Secondary Eclipses of Qatar-1b. *ArXiv e-prints*
- Gibson NP, Aigrain S, Pollacco DL et al (2010) Ground-based detection of thermal emission from the exoplanet WASP-19b. *MNRAS*404:L114–L118
- Gillon M, Demory BO, Triaud AHMJ et al (2009) VLT transit and occultation photometry for the bloated planet CoRoT-1b. *A&A*506:359–367
- Gillon M, Lanotte AA, Barman T et al (2010) The thermal emission of the young and massive planet CoRoT-2b at 4.5 and 8 μm . *A&A*511:A3
- Grillmair CJ, Charbonneau D, Burrows A et al (2007) A Spitzer Spectrum of the Exoplanet HD 189733b. *ApJ*658:L115–L118
- Grillmair CJ, Burrows A, Charbonneau D et al (2008) Strong water absorption in the dayside emission spectrum of the planet HD189733b. *Nature*456:767–769
- Hardy RA, Harrington J, Hardin MR et al (2017) Secondary Eclipses of HAT-P-13b. *ApJ*836:143
- Heng K Demory BO (2013) Understanding Trends Associated with Clouds in Irradiated Exoplanets. *ApJ*777:100
- Henry GW, Marcy GW, Butler RP Vogt SS (2000) A Transiting “51 Peg-like” Planet. *ApJ*529:L41–L44
- Huber KF, Czesla S Schmitt JHMM (2017) Discovery of the secondary eclipse of HAT-P-11 b. *A&A*597:A113
- Irwin JB (1959) Standard light-time curves. *AJ*64:149
- Jansen T Kipping D (2017) Kepler’s Dark Worlds: a Low Albedo for an Ensemble of Neptunian and Terran Exoplanets. *ArXiv e-prints*
- Kammer JA, Knutson HA, Line MR et al (2015) Spitzer Secondary Eclipse Observations of Five Cool Gas Giant Planets and Empirical Trends in Cool Planet Emission Spectra. *ApJ*810:118
- Kilpatrick BM, Lewis NK, Kataria T et al (2017) Spitzer Secondary Eclipse Depths with Multiple Intrapixel Sensitivity Correction Methods Observations of WASP-13b, WASP-15b, WASP-16b, WASP-62b, and HAT-P-22b. *AJ*153:22
- Kipping DM Spiegel DS (2011) Detection of visible light from the darkest world. *MNRAS*417:L88–L92
- Knutson HA, Charbonneau D, Allen LE et al (2007a) A map of the day-night contrast of the extrasolar planet HD 189733b. *Nature*447:183–186
- Knutson HA, Charbonneau D, Deming D Richardson LJ (2007b) A Ground-based Search for Thermal Emission from the Exoplanet TrES-1. *PASP*119:616–622
- Knutson HA, Charbonneau D, Allen LE, Burrows A Megeath ST (2008) The 3.6–8.0 μm Broadband Emission Spectrum of HD 209458b: Evidence for an Atmospheric Temperature Inversion. *ApJ*673:526–531
- Knutson HA, Charbonneau D, Burrows A, O’Donovan FT Mandushev G (2009a) Detection of A Temperature Inversion in the Broadband Infrared Emission Spectrum of TrES-4. *ApJ*691:866–874
- Knutson HA, Charbonneau D, Cowan NB et al (2009b) The 8 μm Phase Variation of the Hot Saturn HD 149026b. *ApJ*703:769–784
- Knutson HA, Charbonneau D, Cowan NB et al (2009c) Multiwavelength Constraints on the Day-Night Circulation Patterns of HD 189733b. *ApJ*690:822–836

- Knutson HA, Madhusudhan N, Cowan NB et al (2011) A Spitzer Transmission Spectrum for the Exoplanet GJ 436b, Evidence for Stellar Variability, and Constraints on Dayside Flux Variations. *ApJ*735:27
- Knutson HA, Lewis N, Fortney JJ et al (2012) 3.6 and 4.5 μm Phase Curves and Evidence for Non-equilibrium Chemistry in the Atmosphere of Extrasolar Planet HD 189733b. *ApJ*754:22
- Komacek TD, Showman AP Tan X (2017) Atmospheric Circulation of Hot Jupiters: Dayside-Nightside Temperature Differences. II. Comparison with Observations. *ApJ*835:198
- Kopal Z (1946) An introduction to the study of eclipsing variables. Harvard Observatory Monographs 6
- Kreidberg L, Bean JL, Désert JM et al (2014) A Precise Water Abundance Measurement for the Hot Jupiter WASP-43b. *ApJ*793:L27
- Krick JE, Ingalls J, Carey S et al (2016) Spitzer IRAC Sparsely Sampled Phase Curve of the Exoplanet Wasp-14B. *ApJ*824:27
- Lanotte AA, Gillon M, Demory BO et al (2014) A global analysis of Spitzer and new HARPS data confirms the loneliness and metal-richness of GJ 436 b. *A&A*572:A73
- Laughlin G, Deming D, Langton J et al (2009) Rapid heating of the atmosphere of an extrasolar planet. *Nature*457:562–564
- Lendl M, Gillon M, Queloz D et al (2013) A photometric study of the hot exoplanet WASP-19b. *A&A*552:A2
- Lewis NK, Knutson HA, Showman AP et al (2013) Orbital Phase Variations of the Eccentric Giant Planet HAT-P-2b. *ApJ*766:95
- Lewis NK, Showman AP, Fortney JJ, Knutson HA Marley MS (2014) Atmospheric Circulation of Eccentric Hot Jupiter HAT-P-2b. *ApJ*795:150
- Lillo-Box J, Barrado D, Figueira P et al (2017) The TROY project: Searching for co-orbital bodies to known planets. I. Project goals and first results from archival radial velocity. *ArXiv e-prints*
- Line MR, Knutson H, Wolf AS Yung YL (2014) A Systematic Retrieval Analysis of Secondary Eclipse Spectra. II. A Uniform Analysis of Nine Planets and their C to O Ratios. *ApJ*783:70
- Line MR, Stevenson KB, Bean J et al (2016) No Thermal Inversion and a Solar Water Abundance for the Hot Jupiter HD 209458b from HST/WFC3 Spectroscopy. *AJ*152:203
- López-Morales M Seager S (2007) Thermal Emission from Transiting Very Hot Jupiters: Prospects for Ground-based Detection at Optical Wavelengths. *ApJ*667:L191–L194
- López-Morales M, Coughlin JL, Sing DK et al (2010) Day-side z'-band Emission and Eccentricity of WASP-12b. *ApJ*716:L36–L40
- Love AEH (1909) Earth, the yielding of the, to disturbing forces. *MNRAS*69:476
- Luger R, Agol E, Kruse E et al (2016) EVEREST: Pixel Level Decorrelation of K2 Light curves. *ArXiv e-prints*
- Luger R, Kruse E, Foreman-Mackey D, Agol E Saunders N (2017) An update to the EVEREST K2 pipeline: Short cadence, saturated stars, and Kepler-like photometry down to $K_p = 15$. *ArXiv e-prints*
- Machalek P, McCullough PR, Burke CJ et al (2008) Thermal Emission of Exoplanet XO-1b. *ApJ*684:1427–1432
- Machalek P, McCullough PR, Burrows A et al (2009) Detection of Thermal Emission of XO-2b: Evidence for a Weak Temperature Inversion. *ApJ*701:514–520
- Machalek P, Greene T, McCullough PR et al (2010) Thermal Emission and Tidal Heating of the Heavy and Eccentric Planet XO-3b. *ApJ*711:111–118
- Majeau C, Agol E Cowan NB (2012) A Two-dimensional Infrared Map of the Extrasolar Planet HD 189733b. *ApJ*747(L20):L20
- Mancini L, Ciceri S, Chen G et al (2013) Physical properties, transmission and emission spectra of the WASP-19 planetary system from multi-colour photometry. *MNRAS*436:2–18
- Martíoli E, Colón KD, Angerhausen D et al (2017) A survey of eight hot Jupiters in secondary eclipse using WIRCam at CFHT. *ArXiv e-prints*
- Maxted PFL, Anderson DR, Doyle AP et al (2013) Spitzer 3.6 and 4.5 μm full-orbit light curves of WASP-18. *MNRAS*428:2645–2660

- Mazeh T, Nachmani G, Sokol G, Faigler S, Zucker S (2012) Kepler KOI-13.01 - Detection of beaming and ellipsoidal modulations pointing to a massive hot Jupiter. *A&A*541:A56
- Mollière P, van Boekel R, Bouwman J et al (2016) Observing transiting planets with JWST – Prime targets and their synthetic spectral observations. *ArXiv e-prints*
- Morley CV, Knutson H, Line M et al (2017) Forward and Inverse Modeling of the Emission and Transmission Spectrum of GJ 436b: Investigating Metal Enrichment, Tidal Heating, and Clouds. *AJ*153:86
- Morris BM, Mandell AM, Deming D (2013) Kepler’s Optical Secondary Eclipse of HAT-P-7b and Probable Detection of Planet-induced Stellar Gravity Darkening. *ApJ*764:L22
- Nymeyer S, Harrington J, Hardy RA et al (2011) Spitzer Secondary Eclipses of WASP-18b. *ApJ*742:35
- O’Donovan FT, Charbonneau D, Harrington J et al (2010) Detection of Planetary Emission from the Exoplanet TrES-2 Using Spitzer/IRAC. *ApJ*710:1551–1556
- O’Rourke JG, Knutson HA, Zhao M et al (2014) Warm Spitzer and Palomar Near-IR Secondary Eclipse Photometry of Two Hot Jupiters: WASP-48b and HAT-P-23b. *ApJ*781:109
- Parmentier V, Fortney JJ, Showman AP, Morley C, Marley MS (2016) Transitions in the Cloud Composition of Hot Jupiters. *ApJ*828:22
- Parviainen H, Deeg HJ, Belmonte JA (2013) Secondary eclipses in the CoRoT light curves. A homogeneous search based on Bayesian model selection. *A&A*550:A67
- Rauer H, Catala C, Aerts C et al (2014) The PLATO 2.0 mission. *Experimental Astronomy* 38:249–330
- Richardson LJ, Deming D, Seager S (2003a) Infrared Observations during the Secondary Eclipse of HD 209458b. II. Strong Limits on the Infrared Spectrum Near 2.2 μ m. *ApJ*597:581–589
- Richardson LJ, Deming D, Wiedemann G et al (2003b) Infrared Observations during the Secondary Eclipse of HD 209458b. I. 3.6 Micron Occultation Spectroscopy Using the Very Large Telescope. *ApJ*584:1053–1062
- Ricker GR (2014) The Transiting Exoplanet Survey Satellite Mission. *Journal of the American Association of Variable Star Observers (JAAVSO)* 42:234
- Rogers JC, Apai D, López-Morales M, Sing DK, Burrows A (2009) Ks-Band Detection of Thermal Emission and Color Constraints to CoRoT-1b: A Low-Albedo Planet with Inefficient Atmospheric Energy Redistribution and a Temperature Inversion. *ApJ*707:1707–1716
- Rostron JW, Wheatley PJ, Anderson DR et al (2014) The thermal emission of the exoplanet WASP-3b. *MNRAS*441:3666–3678
- Rowe JF, Matthews JM, Seager S et al (2008) The Very Low Albedo of an Extrasolar Planet: MOST Space-based Photometry of HD 209458. *ApJ*689:1345–1353
- Sanchis-Ojeda R, Rappaport S, Winn JN et al (2013) Transits and Occultations of an Earth-sized Planet in an 8.5 hr Orbit. *ApJ*774:54
- Santerne A, Bonomo AS, Hébrard G et al (2011) SOPHIE velocimetry of Kepler transit candidates. IV. KOI-196b: a non-inflated hot Jupiter with a high albedo. *A&A*536:A70
- Sato B, Hirano T, Omiya M et al (2015) Precise Radial Velocity Measurements for Kepler Giants Hosting Planetary Candidates: Kepler-91 and KOI-1894. *ApJ*802:57
- Schwartz JC, Cowan NB (2015) Balancing the energy budget of short-period giant planets: evidence for reflective clouds and optical absorbers. *MNRAS*449:4192–4203
- Schwartz JC, Kashner Z, Jovmir D, Cowan NB (2017) Phase Offsets and the Energy Budgets of Hot Jupiters. *ApJ*850:154
- Sheets HA, Deming D (2017) Average Albedos of Close-in Super-Earths and Super-Neptunes from Statistical Analysis of Long-cadence Kepler Secondary Eclipse Data. *AJ*154:160
- Sheppard KB, Mandell AM, Tamburo P et al (2017) Evidence for a Dayside Thermal Inversion and High Metallicity for the Hot Jupiter WASP-18b. *ApJ*850:L32
- Showman AP, Guillot T (2002) Atmospheric circulation and tides of “51 Pegasus b-like” planets. *A&A*385:166–180
- Shporer A, Hu R (2015) Studying Atmosphere-dominated Hot Jupiter Kepler Phase Curves: Evidence that Inhomogeneous Atmospheric Reflection Is Common. *AJ*150:112

- Shporer A, O'Rourke JG, Knutson HA et al (2014) Atmospheric Characterization of the Hot Jupiter Kepler-13Ab. *ApJ*788:92
- Sing DK, López-Morales M (2009) Ground-based secondary eclipse detection of the very-hot Jupiter OGLE-TR-56b. *A&A*493:L31–L34
- Smith AMS, Anderson DR, Skillen I, Collier Cameron A, Smalley B (2011) Thermal emission from WASP-33b, the hottest known planet. *MNRAS*416:2096–2101
- Smith AMS, Anderson DR, Madhusudhan N et al (2012) Thermal emission from WASP-24b at 3.6 and 4.5 μm . *A&A*545:A93
- Snellen IAG (2005) High-precision K-band photometry of the secondary eclipse of HD 209458. *MNRAS*363:211–215
- Snellen IAG, Covino E (2007) K-band transit and secondary eclipse photometry of exoplanet OGLE-TR-113b. *MNRAS*375:307–312
- Snellen IAG, de Mooij EJW, Albrecht S (2009) The changing phases of extrasolar planet CoRoT-1b. *Nature*459:543–545
- Snellen IAG, de Mooij EJW, Burrows A (2010) Bright optical day-side emission from extrasolar planet CoRoT-2b. *A&A*513:A76
- Stevenson KB, Harrington J, Nymeyer S et al (2010) Possible thermochemical disequilibrium in the atmosphere of the exoplanet GJ 436b. *Nature*464:1161–1164
- Stevenson KB, Harrington J, Fortney JJ et al (2012) Transit and Eclipse Analyses of the Exoplanet HD 149026b Using BLISS Mapping. *ApJ*754:136
- Stevenson KB, Bean JL, Madhusudhan N, Harrington J (2014a) Deciphering the Atmospheric Composition of WASP-12b: A Comprehensive Analysis of its Dayside Emission. *ApJ*791:36
- Stevenson KB, Désert JM, Line MR et al (2014b) Thermal structure of an exoplanet atmosphere from phase-resolved emission spectroscopy. *Science* 346:838–841
- Stevenson KB, Line MR, Bean JL et al (2017) Spitzer Phase Curve Constraints for WASP-43b at 3.6 and 4.5 μm . *AJ*153:68
- Swain MR, Tinetti G, Vasisht G et al (2009a) Water, Methane, and Carbon Dioxide Present in the Dayside Spectrum of the Exoplanet HD 209458b. *ApJ*704:1616–1621
- Swain MR, Vasisht G, Tinetti G et al (2009b) Molecular Signatures in the Near-Infrared Dayside Spectrum of HD 189733b. *ApJ*690:L114–L117
- Swain MR, Deroo P, Griffith CA et al (2010) A ground-based near-infrared emission spectrum of the exoplanet HD189733b. *Nature*463:637–639
- Todorov K, Deming D, Harrington J et al (2010) Spitzer IRAC Secondary Eclipse Photometry of the Transiting Extrasolar Planet HAT-P-1b. *ApJ*708:498–504
- Todorov KO, Deming D, Knutson HA et al (2012) Warm Spitzer Observations of Three Hot Exoplanets: XO-4b, HAT-P-6b, and HAT-P-8b. *ApJ*746:111
- Todorov KO, Deming D, Knutson HA et al (2013) Warm Spitzer Photometry of Three Hot Jupiters: HAT-P-3b, HAT-P-4b and HAT-P-12b. *ApJ*770:102
- Todorov KO, Deming D, Burrows A, Grillmair CJ (2014) Updated Spitzer Emission Spectroscopy of Bright Transiting Hot Jupiter HD 189733b. *ApJ*796:100
- Triaud AHMJ (2014) Colour-magnitude diagrams of transiting Exoplanets - I. Systems with parallaxes. *MNRAS*439:L61–L64
- Triaud AHMJ, Lanotte AA, Smalley B, Gillon M (2014) Colour-magnitude diagrams of transiting Exoplanets - II. A larger sample from photometric distances. *MNRAS*444:711–728
- Triaud AHMJ, Gillon M, Ehrenreich D et al (2015) WASP-80b has a dayside within the T-dwarf range. *MNRAS*450:2279–2290
- von Essen C, Mallonn M, Albrecht S et al (2015) A temperature inversion in WASP-33b? Large Binocular Telescope occultation data confirm significant thermal flux at short wavelengths. *A&A*584:A75
- Walker G, Matthews J, Kuschnig R et al (2003) The MOST Asteroseismology Mission: Ultra-precise Photometry from Space. *PASP*115:1023–1035
- Wang W, van Boekel R, Madhusudhan N et al (2013) Ground-based Detections of Thermal Emission from the Dense Hot Jupiter WASP-43b in the H and K_s Bands. *ApJ*770:70

- Welsh WF, Orosz JA, Seager S et al (2010) The Discovery of Ellipsoidal Variations in the Kepler Light Curve of HAT-P-7. *ApJ*713:L145–L149
- Wheatley PJ, Collier Cameron A, Harrington J et al (2010) The thermal emission of the exoplanets WASP-1b and WASP-2b. *ArXiv e-prints*
- Wilkins AN, Delrez L, Barker AJ et al (2017) Searching For Rapid Orbital Decay of WASP-18b. *ArXiv e-prints*
- Williams PKG, Charbonneau D, Cooper CS, Showman AP Fortney JJ (2006) Resolving the Surfaces of Extrasolar Planets with Secondary Eclipse Light Curves. *ApJ*649:1020–1027
- Winn JN, Holman MJ, Shporer A et al (2008) The Transit Light Curve Project. VIII. Six Occultations of the Exoplanet TrES-3. *AJ*136:267–271
- Wong I, Knutson HA, Lewis NK et al (2015) 3.6 and 4.5 μm Phase Curves of the Highly Irradiated Eccentric Hot Jupiter WASP-14b. *ApJ*811:122
- Wong I, Knutson HA, Kataria T et al (2016) 3.6 and 4.5 μm Spitzer Phase Curves of the Highly Irradiated Hot Jupiters WASP-19b and HAT-P-7b. *ApJ*823:122
- Zellem RT, Griffith CA, Deroo P, Swain MR Waldmann IP (2014a) The Ground-based H-, K-, and L-band Absolute Emission Spectra of HD 209458b. *ApJ*796:48
- Zellem RT, Lewis NK, Knutson HA et al (2014b) The 4.5 μm Full-orbit Phase Curve of the Hot Jupiter HD 209458b. *ApJ*790:53
- Zhao M, Milburn J, Barman T et al (2012a) Detection of K_S -band Thermal Emission from WASP-3b. *ApJ*748:L8
- Zhao M, Monnier JD, Swain MR, Barman T Hinkley S (2012b) Ground-based Detections of Thermal Emission from CoRoT-1b and WASP-12b. *ApJ*744:122
- Zhao M, O'Rourke JG, Wright JT et al (2014) Characterization of the Atmosphere of the Hot Jupiter HAT-P-32Ab and the M-dwarf Companion HAT-P-32B. *ApJ*796:115
- Zhou G, Kedziora-Chudczer L, Bayliss DDR Bailey J (2013) Examining the Broadband Emission Spectrum of WASP-19b: A New z-band Eclipse Detection. *ApJ*774:118
- Zhou G, Bayliss DDR, Kedziora-Chudczer L et al (2014) K_s -band secondary eclipses of WASP-19b and WASP-43b with the Anglo-Australian Telescope. *MNRAS*445:2746–2757
- Zhou G, Bayliss DDR, Kedziora-Chudczer L et al (2015) Secondary eclipse observations for seven hot-Jupiters from the Anglo-Australian Telescope. *MNRAS*454:3002–3019